OVERALL RESPONSE OF 2-PLY LAMINATED GLASS PLATES UNDER OUT-OF-PLANE LOADING

Luigi Biolzi, Marco Simoncelli
Department of Architecture, Built Environment and Construction Engineering
Politecnico di Milano, Milano-Italy

Abstract

The results of an experimental and numerical investigation on the mechanical response of undamaged and damaged 2-ply Laminated Glass (LG) plates with different interlayers are presented in the paper. Three different interlayers, polyvinyl butyral (PVB), SentryGlas (SG) and Saflex DG41 (DG41) characterized by different rheological properties and fully tempered glass plates were considered. Simply supported plates under out of plane loads were tested in three different configurations: configuration 0, undamaged; configuration I, partially damaged, with a broken ply below (bottom ply) and configuration II, partially damaged, with a broken ply above (top ply). In the three configurations the top ply is always subjected to compression while the bottom one is in tension. The main aspects and the different response of each configuration were discussed and compared. Experimental results highlighted the influence of the interlayer properties on both the pre- and post-breakage behavior. Moreover, numerical models were developed to reproduce the experimental results. For the post-breakage response two different strategies were developed: a) the equivalent temperature variation and b) elastic-brittle constitutive law. Differences and advantages associated with both solutions are discussed. Finally, extensive parametric numerical analyses are proposed to underline the influence on the mechanical response of different parameters: i) plate geometry (size effect); ii) interlayer thickness; iii) glass thickness; iv) additional glass ply (3-ply LG plate). It is underlined that the size effect plays an important role on the mechanical response of LG plates and it should be always considered in the design. The numerical findings were used to define a critical length from which the plates behave as monolithic, independently of the stiffness of the interlayer.

Keywords: *Laminated glass plates, post-breakage behavior, different interlayers, parametric analyses, size effect, numerical modelling*

1.Introduction

As a consequence of the technological progress and the advancement in the field of materials science, contemporary architectural transparency is today a reality of considerable importance. Glass plates, subjected to out-of-plane loading are often employed for floors, roofs, balustrades or façades [1]. Due to the intrinsic brittleness of glass, the design of structural elements needs special requirements to realize robustness and reduce the risk of catastrophic collapse. Consequently, the glass that has relevance in the construction industry is often of a safe type; in particular laminated glass (LG) is selected, which is a composite obtained by two or more glass layers bonded together by polymeric film. The interlayer in the undamaged phase generates shear stress between two connected layers of glass, whereas, in the post-glass breakage range, the polymer confers cohesion to the composite, preventing a catastrophic collapse (Fig. 1). The overall mechanical response of a LG sheet is strongly affected by the temperature and duration of the applied load, as well as delamination phenomena that may occur between the interlayer and glass. Thus, the design of structural and non-structural glass elements should consider both the pre- and post-breakage phase [2].

Figure 1. Fractured laminated tempered glass.

However, there is a lack of systematic experimental studies that give a relative certainty on the actual structural response, so it is necessary to conduct tests in the framework of the *design-by-testing* rule [3]. The response in the post failure range is also affected by the bridging between adjacent glass pieces that is made possible by the polymer [4]. Therefore, stiffness of the interlayer and debonding of the glass-interlayer interface are factors that influence the post-breakage response [5-8]. Commonly used polymeric films for glass lamination are: Polyvinyl Butyral (PVB) [9,10], SentryGlas (SG) [11], and Ethylene Vinyl Acetate (EVA) [12]. PVB necessitates the supplement of softeners that provide plasticity and toughness. SG is an ionoplast polymer principally created with ethylene/methacrylic acid copolymers with metal salts in modest quantities. In comparison to the PVB, SG exhibits elevated stiffness even at very small strains. The properties of EVA may vary from partial crystalline and thermoplastic to amorphous and rubber-like, but an increased quantity of vinyl acetate improves both strength and stiffness capacity. DG41, commercially known as Eastman Saflex DG41 (www.saflex.com), is a toughened PVB. Unlike PVB, it shows significant stiffness even at very small strains, which is the field of interest for structural applications.

In this paper, the post-breakage response of 2-ply simply supported LG plates under out-of-plane loading was investigated through experiments at different damage arrangements. The considered plates were made by 2-ply tempered (T) glass and three different interlayer films: PVB, DG41, or SG. Three different configurations were considered: i) configuration 0, undamaged laminated glass plates (UDLG); ii) configuration I, partially damaged laminated glass (PDLG) with the broken ply below (bottom ply); iii) configuration II, PDLG with the broken ply above (top ply). In the UDLG configuration, the load was increased until the collapse of the bottom glass ply. Then, in the other two different PDLG configurations the global failure was reached. In particular, the influence of the interlayers on the pre- and post-failure phase is illustrated and discussed. It should be remarked that, in the three configurations, the top ply is always subjected to compression while the bottom one is in tension. The experimental findings were modeled and compared with finite element (FE) analyses.

In particular, the post-breakage behavior was simulated using two different strategies: the use of an equivalent temperature and the implementation of an elastic-brittle constitutive law. Finally, parametric analyses were developed to study the influence of different parameters on the LG plates response, such as: i) size effect; ii) thickness of the glass and interlayer; iii) additional ply of glass (3-ply LG plate). The parametric studies were used to define a *critical length* from which the considered plates behave as *monolithic*, independently of the interlayer material. The present paper brings additional important information for the design of LG plates with different interlayers. It is underlined the importance of the post-failure response of the glass elements which is directly connected to interlayer and glass types [13].

2. Interlayers characterization

A strong background on the characteristics of the interlayers is of paramount importance to understand clearly the overall response of LG plates [14]. The short-term tensile mechanical properties of a material are generally the reference and most important properties considered to characterize the material itself.

To perform uniaxial tensile tests, *dog-bone* shaped specimens were obtained from a sheet of interlayer as required in [15]. During the tests the strain was measured taking as a reference two points located at a predefined distance. Tests were executed in a room with controlled humidity and temperature and different constant displacement rate were selected: i) 5 mm/min; ii) 50 mm/min; iii) 500 mm/min. Engineering stresses and strains are depicted in Fig. 2. The failure was always observed in a section within the narrow area, never in the grips nor in the interface with clamps. The maximum tensile value was associated with very high strains which generally did not governs the design of laminated glass elements. Furthermore, the response of the three interlayer was completely different to one another. DG41 and SG are characterized by an initial high stiffness whit an important decrement after a local maximum point (which for other traditional materials is general indicate as a yielding point).

On the contrary PVB showed an increasing stiffness with the increase of the strains, without any abrupt change in the slope of the curve.

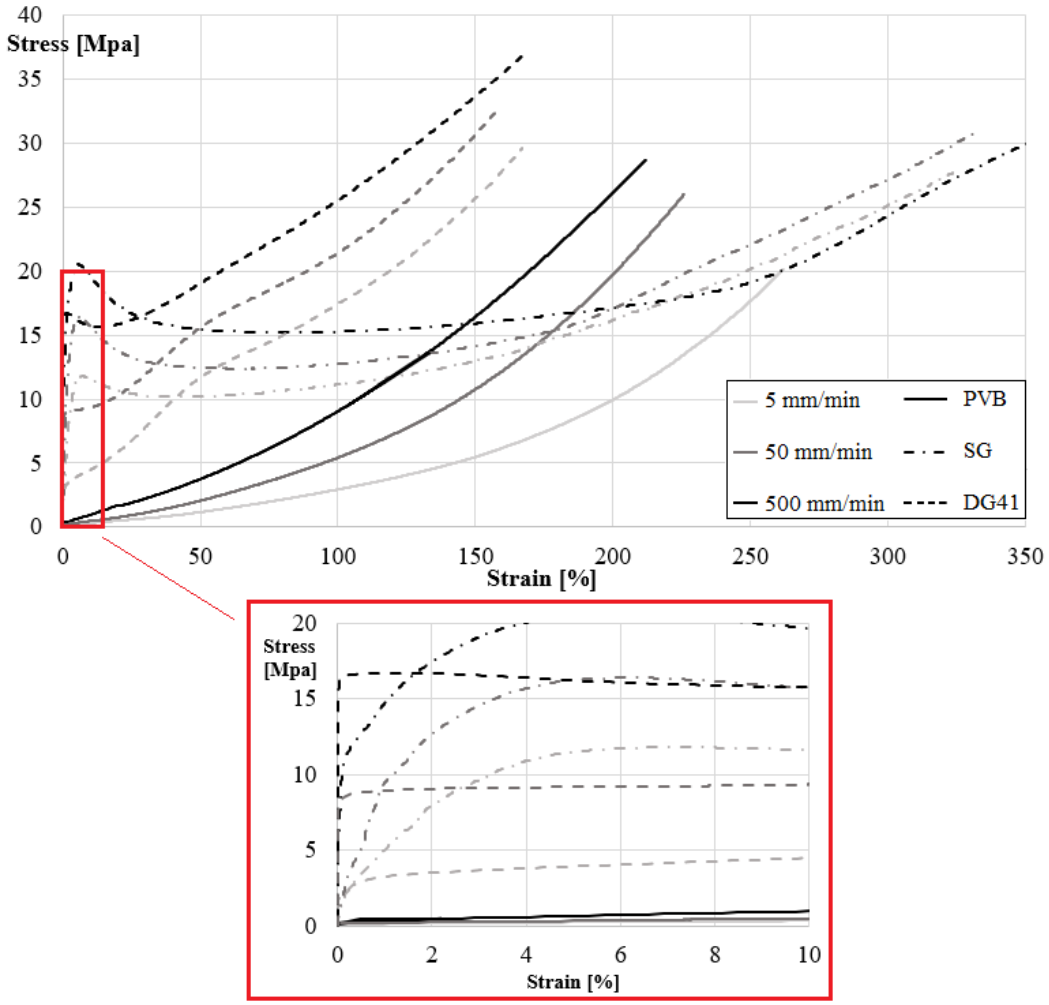

Figure 2. Engineering stress- stain diagrams for DG41, PVB and SG

To identify the elastic modulus the current standard, suggest the use of the so-called *chord slope method* [16]: two points should be identified in the initial part of the stress-stain graphs which are assumed as the elastic part of the non-linear response. These points are identified with A and B and are relative to the 0.05% and 0.25% of the strain, respectively. In particular the elastic modulus of the interlayer (E_t) can be evaluated with the equation:

$$E_t = \frac{\sigma_B - \sigma_A}{\varepsilon_B - \varepsilon_A} \quad (1)$$

For the sake of clarity, the estimation of E_t for the three tested materials, with displacement rate equal to 5 mm/min, is depicted in Fig. 3. The solid black line represents the evaluation of E_t in according to the *chord slope method*. It can be noted that only with the SG the black line is quite representative of the initial behavior of the material. PVB and DG41 exhibit a very stiff response, in the 0.05-0.25% strain range, qualitatively similar to the one associated with the SG. However, this response cannot be considered as representative of the material elastic behavior, being immediately followed by a great stiffness reduction. Therefore, to evaluate properly the elastic response of PVB and DG41, the elastic modulus was estimated exactly after the very stiff initial peak, shifting points A and B to 0.5% and 2.5% strain, respectively (dashed black line in Fig. 3).

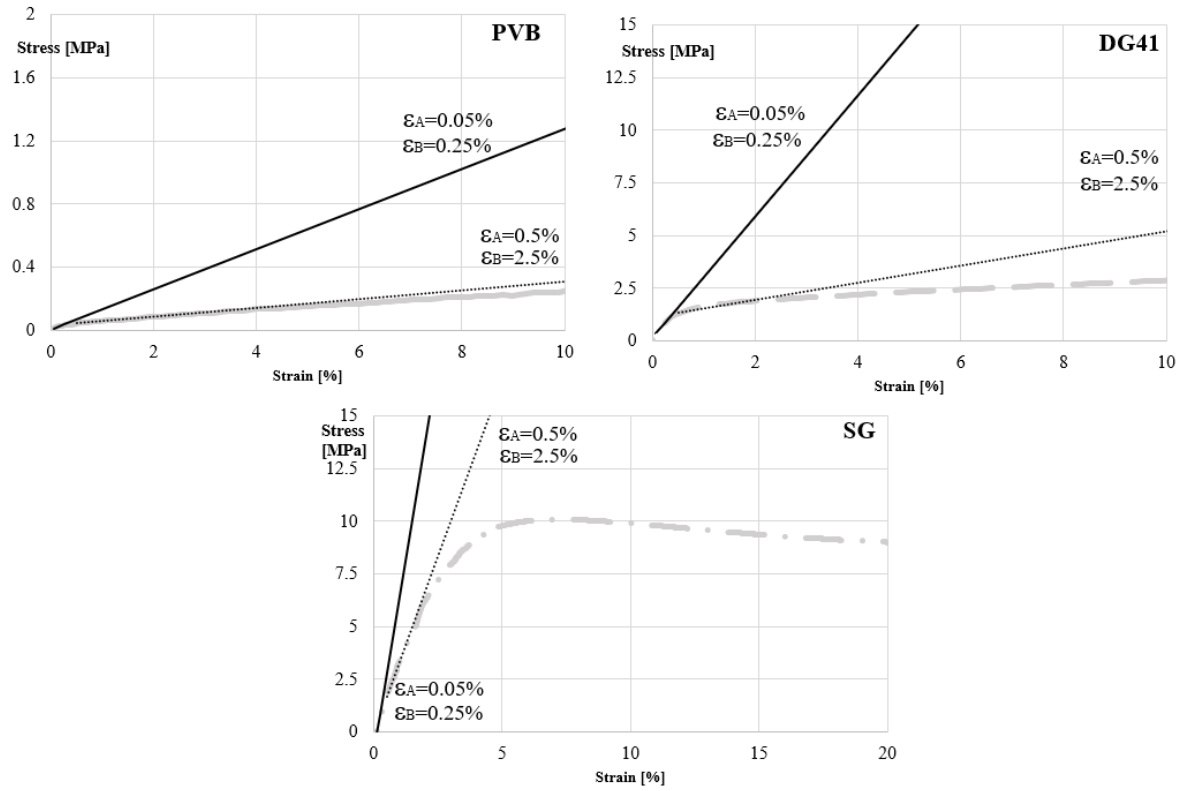

Figure 3. Evaluation of the Elastic modulus of the interlayers (displacement rate 5mm/min).

The results, obtained as a median value between three nominally equal specimens, were reported in Tab. 1 for all the considered displacement ratios.

Table 1. Median elastic modulus, E_t, of the considered interlayers [MPa].

displacement rate	SG	DG41	PVB
5 mm/min	430	52	2.02
50 mm/min	435	163	2.67
500 mm/min	1060	168	4.48

It is confirmed that, for all the considered test velocities, PVB showed a greater flexibility with respect the other two materials. It can be remarked that, for the simulation of experimental tests on LG plates with static or quasi-static loads, like the ones presented in the following sections, the first two rows of Tab. 1 should be considered; otherwise, when impact loads are applied, the third row is the most representative. As expected, for all the three materials the modulus is greatly lower than the one associated with the glass.

The producers (SG, www.kuraray.com; DG41, www.saflex.com; PVB, www.dupont.com) suggested a value of the Poisson ratio, v, equal to v= 0.47 for all the interlayers.

Finally, to proceed with a comprehensive characterization of a polymer it is required to know the response of a material over a long period of time. Because long-term experiments can be troublesome and very expensive a simplified method can be determined for the use of this data in the design, based on short tests with different temperature. Since the equal effect of time and temperature, experimental data at different temperatures can be superposed on data taken at a specified reference temperature by shifting different curves one at a time and consecutively along the *log t* axis about the reference temperature. This time–temperature superposition procedure has the consequence of generating a single curve of shear modulus values (G) expanding over long periods of *log t* at the reference temperature. The final assembled curve is defined as the master curve. Following the time-shift procedure with the Prony series for viscoelastic models together with the Williams-Landel-Ferry coefficients for time-temperature superposition [17], it is possible to obtain the master curves depicted in Fig. 4, in which in the vertical axis is reported the modulus G in MPa. The master curves confirm how the stiffness of all tested materials decreases over time, but at dissimilar rates. The interlayer SG

showed a behavior which is less affected by load duration and temperature changes. The load duration tends to reduce the differences between the DG41 and PVB.

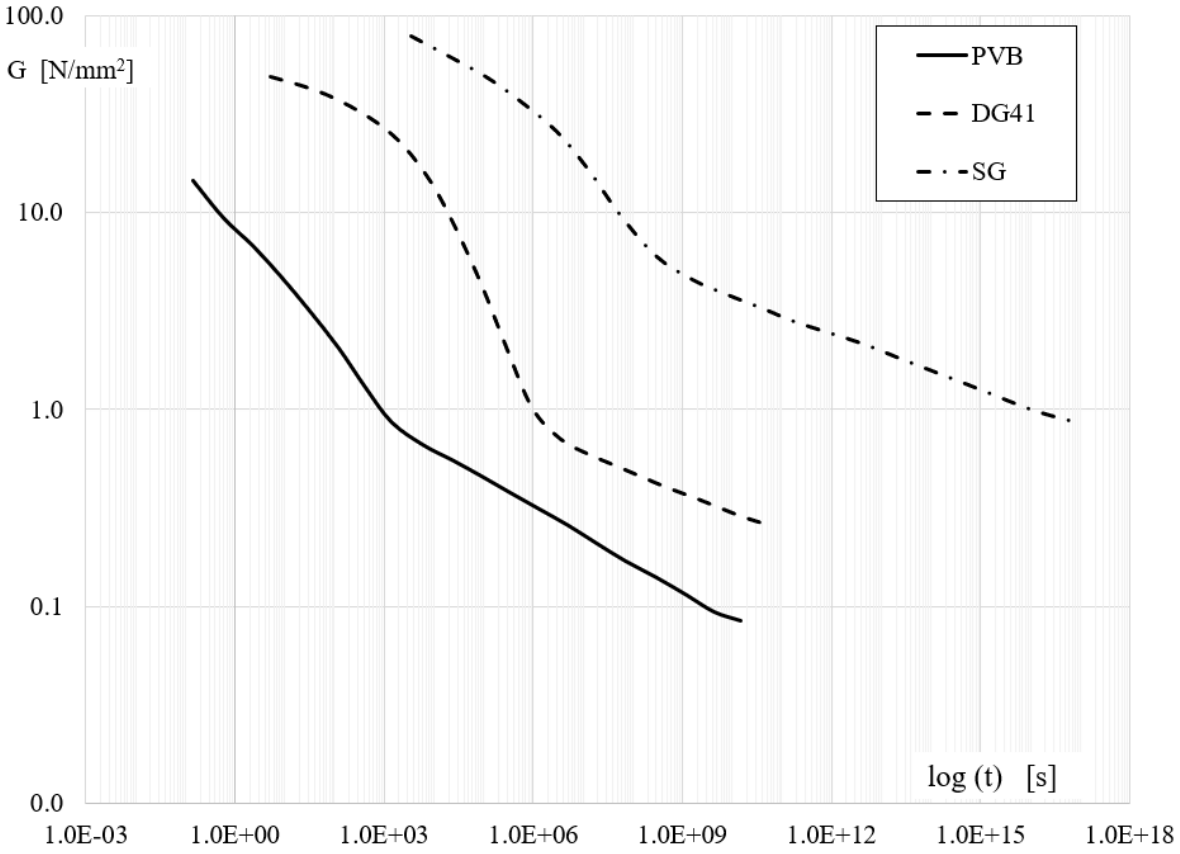

Figure 4. Master curves DG41, PVB and SG.

The obtained results are in agreement with the technical sheets offered by the producers of the materials: SG, www.kuraray.com; DG41, www.saflex.com; PVB, www.dupont.com.

3. Test setup and specimens description

Experimental tests were performed on simply supported LG plates. The specimens were characterized by 2-ply tempered (T) glass with an intermediate polymeric film. The scope of the tests was to monitor the post-failure behavior, starting from the undamaged cases (UDLG) down through the partially damaged ones (PDLG). As reported in Fig. 5, simply support plates were tested with a specimen length equal to 1000 mm x 1100mm. Geometrical similar plates were tested also in cantilever

configuration under a distributed load on its free end [18]. The specimens were manufactured by different interlayer material: PVB, DG41, and SG.

Both ends of the plates were simply supported on steel rollers located along a steel beam, close to the glass end, that hampered vertical displacements but permitted the rotation. An incremental load was applied in the middle of the plate by means of a Hydraulic jack connected to a longitudinal steel beam which was directly in contact with the upper surface of the plates. Vertical displacements were monitored continuously by means of two linear variable displacement transducer (LVTD) sensors located in the middle-section, at left and right ends of the plate.

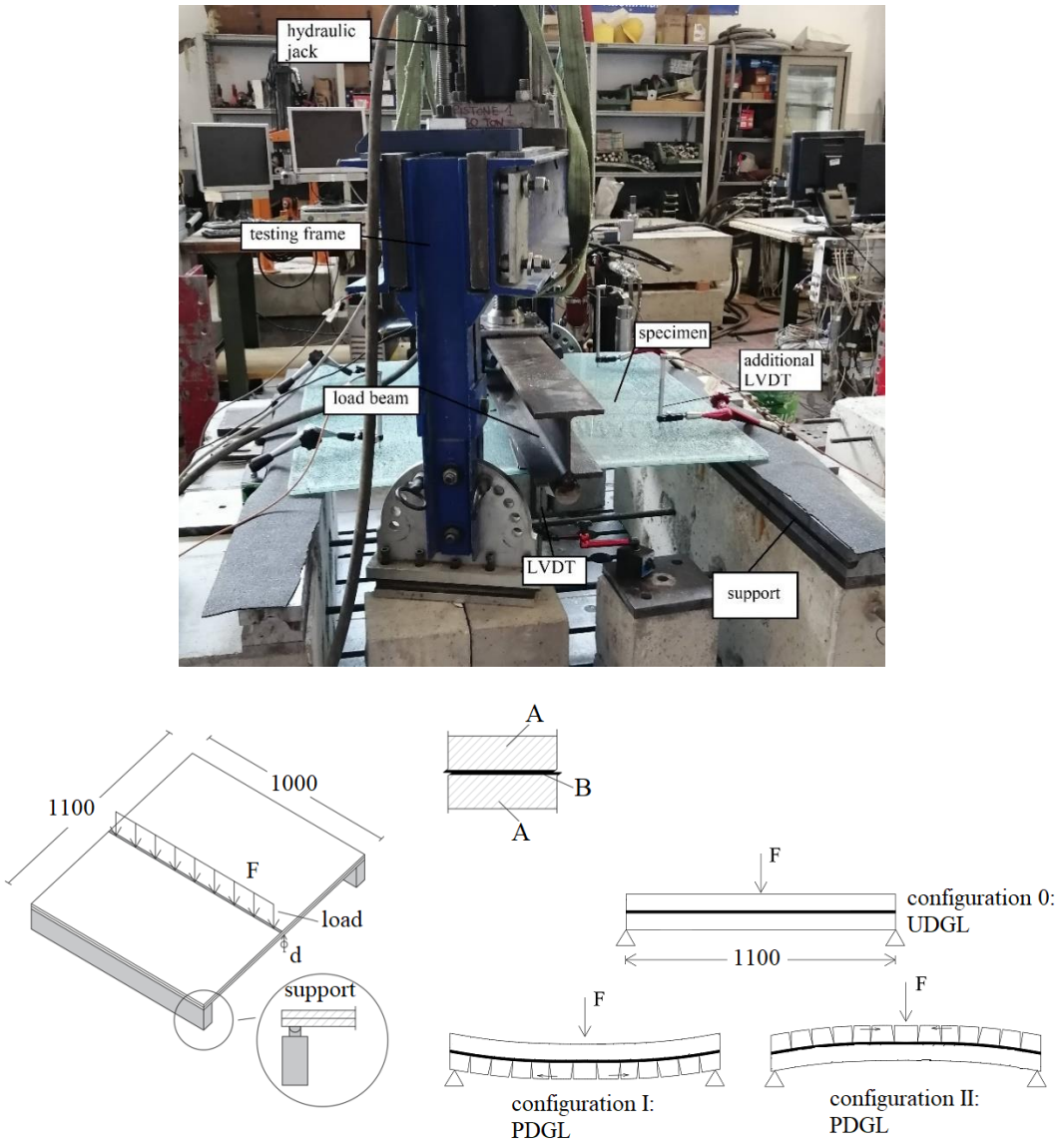

Figure 5. The considered test setup.

In Tab. 2 all the tested plates are reported together with the thickness of the glass plies and of the interlayer.

Table 2. Considered specimen for tests.

specimen name	Layer A	Layer B
8TPVB	TG – 8mm	PVB 1.52mm
8TDG	TG – 8mm	DG41 1.52mm
8TSG	TG – 8mm	SG 0.89mm
10TSG	TG – 10mm	SG 0.89mm

The thickness of 8mm (or 10mm) for the glass plies is to be intended as the commercial thickness. The actual thickness was evaluated with a calibre, repeating the measure on more than ten different points, showing a difference between the actual and the nominal value less than 5%. Different configurations were tested (Fig. 5):

- configuration 0 (UDLG): vertical load was increased until the collapse of the bottom glass ply;
- configuration I (bottom PDLG): PDLG specimens were tested with the damaged glass ply located at the bottom. In this damaged configuration the load was increased until the global collapse;
- configuration II (top PDLG): PDLG specimens were tested with the damaged glass ply located at the top. In this damaged configuration the load was increased until the global collapse.

As discussed in the following, the mechanical response of LG plates varies significantly, depending on which ply fails first: if the ply on top fails first (simulated in configuration II), an increasing load induces compressive effects among fragments and reduces the amplitude of cracks. Vice-versa, if the bottom ply fails (simulated in configuration I), the increasing vertical load increases the distance between fragments.

3.1. Results for configuration 0, UDLG

The behavior of UDLG specimens was approximately linear and strictly depended on the elastic modulus (and thickness) of the glass and of the interlayer. Results associated with the experimental tests on UDGL, are reported in Tab. 3, in terms of load value which generated cracks in the bottom ply, F_0 and the associate displacement (i.e. displacement at the ultimate limit state, d_{ULS}). Moreover, the residual deformation (res. def.) obtained after the completely load removal is reported, together with the slope of the force-displacement response.

Table 3. Results obtained on UDLG specimens.

specimen name	F_0 [kN]	d_{ULS} [mm]	res. def. [mm]	slope
8TPVB	20.0	49.2	6.6	0.40
8TDG	27.5	25.7	6.9	1.08
8TSG	34.3	34.5	6.9	0.99
10TSG	48.5	24.6	6.5	1.97

A direct comparison can be made between PVB and DG41 interlayer by comparing 8TPVB with 8TDG. Due to its higher stiffness 8TDG reached a failure load 1.4 times greater and to an almost 3 times greater stiffness. Moreover, the influence of glass thickness on the pre-breakage response can be appreciated by comparing 8TSG with 10TSG specimens. As expected, since the glass thickness was 1.25 times higher, 10TSG was 2 times more rigid and 1.5 more strength than the 8TSG. LG plates made by SG and DG41 have similar response: the higher thickness of the DG41 interlayer compensate the quite lower elastic modulus.

After the breakage of the bottom ply the load suddenly decreased and when it was completely removed, a permanent deformation of the plates was always registered independently of the interlayer type and glass thickness. This peculiar aspect will be discussed in detail in the following section 4.2. The broken bottom glass ply in configuration 0, is reported in Fig. 6 for the 8TDG and 8TPVB specimens. A zoom on the crack to appreciate the dimension of the fragments is also proposed. As expected, tempered glass ply broke into a great number of small pieces (Fig. 6) uniformly distributed

along the ply itself. In all the tested specimens, the first crack was always detected along the middle line (below the load beam), in different positions.

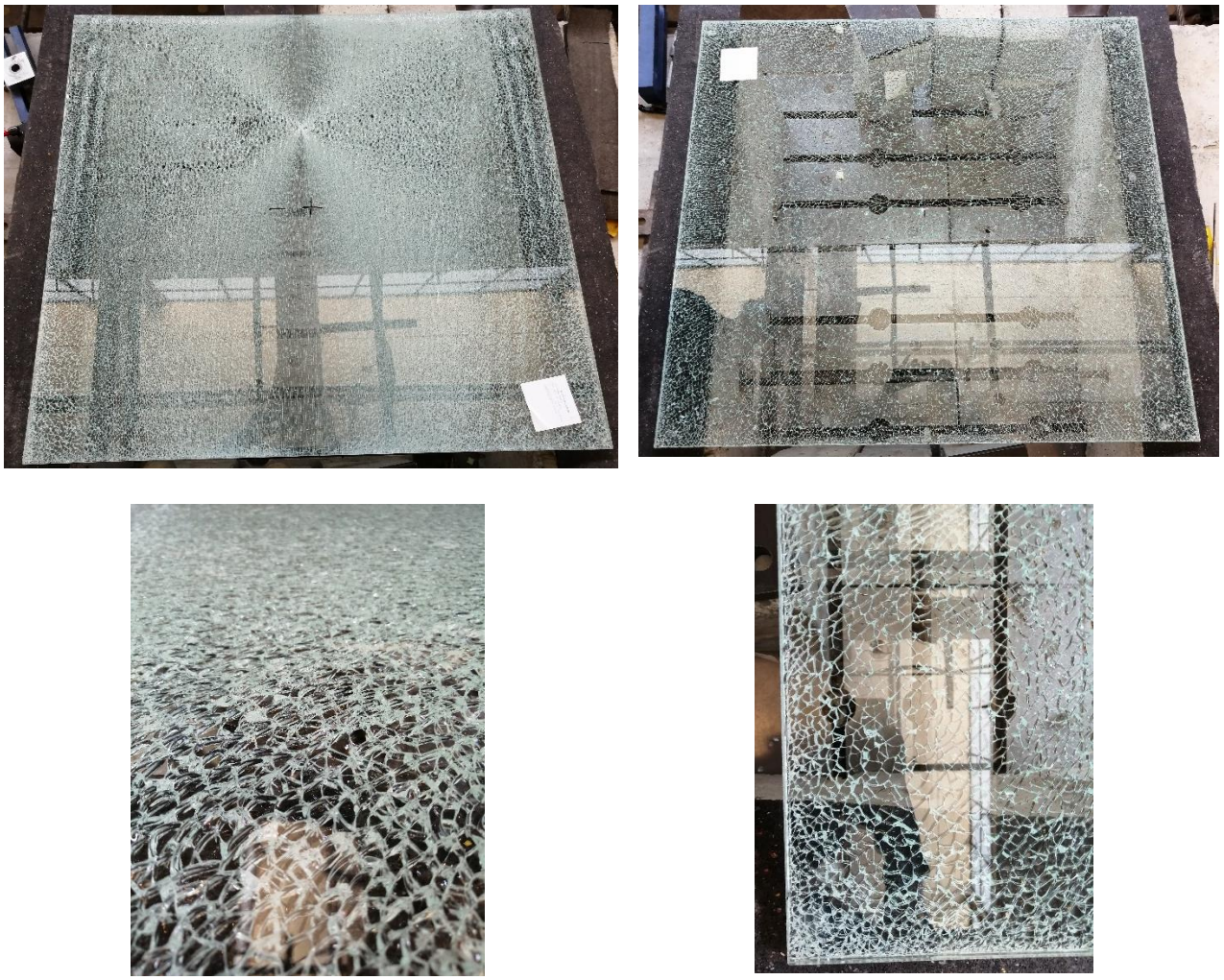

a) b)

Figure 6. Picture of a damaged bottom ply glass for: a) 8TDG and b) 8TPVB specimen

Among the different methods proposed in literature to predict the pre-breakage behavior (see e.g. [19-21]) the so-called Enhanced Effective Thickness (EET) approach was selected, which is the one suggested also in [2]. Starting from the definition of the number of layers, type of interlayer, geometry of the specimen and the boundary conditions, equivalent thickness were estimated. In particular, the considered cases should be assumed equivalent to a simply supported beam with a concentrated load

in the middle. The equivalent thickness, $\hat{h}_w$, used to calculate the maximum displacement in the middle is strictly depended on the non-dimensional factor η, and is equal to:

$$\hat{h}_w = \sqrt[3]{\frac{1}{\frac{\eta}{\sum_{i=1}^{N} h_i^3 + 12\sum_{i=1}^{N}(h_i d_i^2)} + \frac{(1-\eta)}{\sum_{i=1}^{N} h_i^3}}} \quad \text{with} \quad \eta = \frac{1}{1 + \frac{E\, h_{int}}{G_{int}\, b}\frac{J_{abs}}{J_{full}} A^x \Psi} \tag{2a,b}$$

where h_i is the thickness of *i-th* glass ply having a young modulus equal to E; h_{int} is the thickness of the internal polymer with a shear modulus equal to G_{int}; A^x is the geometric area; J_{full} and J_{abs} are the second moment of area related to the *monolithic* and *layered* limit, respectively. Finally, Ψ is a coefficient which directly depends on the boundary conditions of the considered case and is reported in ref. [2]. G_{int}; is directly related to the elastic modulus of the interlayer, E_t, discussed in the previous section 2. By looking to eq. (2b) it can be remarked that when $G_{int} = \infty$ (*monolithic limit*) terms η is equal to 1, on the contrary if $G_{int} = 0$ (*layered limit*) terms η becomes 0.

On the other hand, the equivalent thickness used to calculate the maximum stresses on the outer faces of the glass plies, $\hat{h}_{i,\sigma}$ can be estimated with :

$$\hat{h}_{i,\sigma} = \sqrt{\frac{1}{\frac{2\,\eta |d_i|}{\sum_{i=1}^{N} h_i^3 + 12\sum_{i=1}^{N}(h_i d_i^2)} + \frac{h_i}{\hat{h}_w^3}}} \tag{2c}$$

In Tab. 4 a comparison between experimental ($d_{ULS,ex}$) and theoretical ($d_{ULS,th}$) maximum displacements is reported together with the maximum tension expected on the bottom glass ply, σ_t.

Table 4. Results obtained on UDLG specimens.

specimen name	F_0 [kN]	$d_{ULS,ex}$ [mm]	$\hat{h}_w$ [mm]	$d_{ULS,th}$ [mm]	$d_{ULS,ex}$ / $d_{ULS,th}$	σ_t [MPa]
8TPVB	20.0	49.2	12.0	51.9	5%	185
8TDG	27.5	25.7	16.8	25.8	1%	170
8TSG	34.3	34.5	16.4	34.8	1%	200
10TSG	48.5	24.6	20.4	25.5	4%	195

Note that for all the cases, the differences are always lower than 5% showing a more than good agreement with experimental results and the ones obtained from the EET method. Moreover, the value of the maximum tension σ_t results quite similar for all the considered specimens, demonstrating that a similar tempering process were performed on all the tested glass plies.

3.2. Results for PDLG

3.2.1 Configuration I

In configuration 0, when the bottom ply broke the load suddenly decreased but the LG plates still had a residual load carrying capacity, producing the configuration I. A lateral view of the damaged ply in this configuration I is reported in Fig. 7. Furthermore, the complete force-displacement curves are sketched in Fig. 8.

Figure 7. Lateral view of configuration I, broken bottom ply.

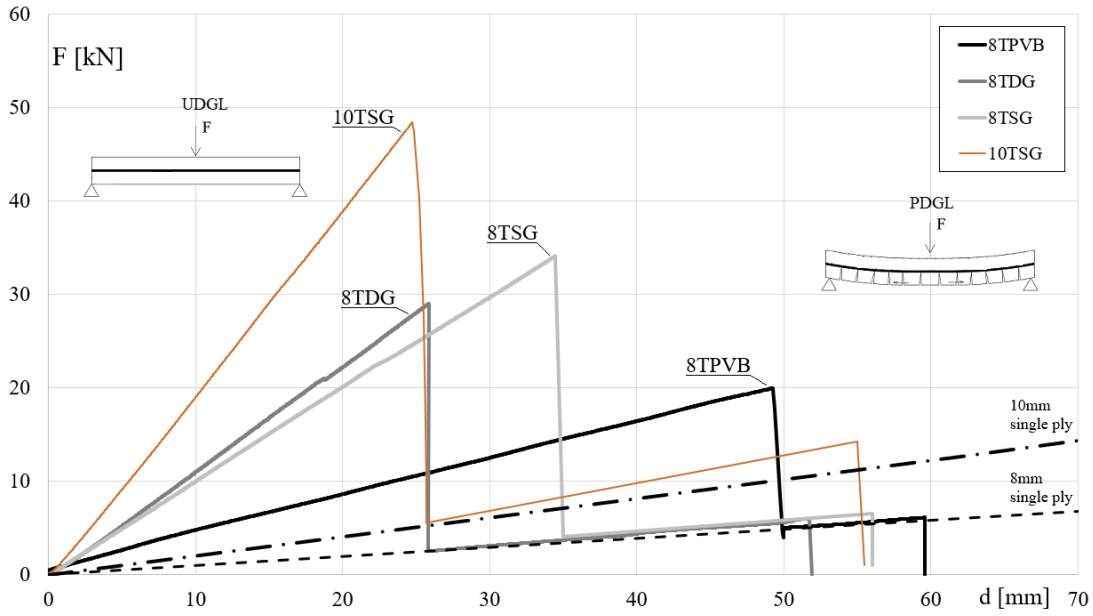

Figure 8. Experimental response in configuration 0 and I.

The global stiffness of the LG plates with the bottom ply cracked is greatly reduced with respect to the UDLG case. From an engineering standpoint, the first breakage of the bottom ply could be intended as an ultimate limit state (ULS) while when both plies crack, a collapse limit state (CLS) is identified. Plates with PVB always showed a limited capacity between ULS and CLS identifying a low post-breakage capacity. On the contrary plates with DG41 and SG showed a huge deformability capacity before the CLS. In the same Fig. 8, with the dashed black line is reported the force-displacement response of a monolithic plate made by only one glass ply (8mm or 10mm of thickness). It can be noted that for all the specimens, the slope of the post-breakage branches is never coincident with the dashed ones. In fact, despite the bottom ply is completely cracked still gives a non-zero contribution on the global stiffness. This contribution is the so-called *tension stiffening* and mainly depends on two factors: i) dimensions of the fragments. The experimental evidence confirms that the greater are the fragments and the stiffer is the plate; ii) stiffness of the interlayer. Stiffer is the interlayer and sligthly higher is the slope of the post-breakage branch. Finally, in Tab. 5 the results associated with configuration I are reported in term of collapse limit state load, F_I and the associated vertical displacement ($d_{CLS,I}$). Moreover, the $d_{CLS,I}/d_{ULS}$ ratio is presented which indicate the post-breakage capacity of the plate. The global failure load F_I ranges from 3.2 to 5.2 times lower than the load registered in the UDGL at the failure of the bottom glass ply, F_0.

Table 5. Results obtained on PDLG specimens.

	UDLG		PDLG, Crack on bottom ply		
specimen name	F_0 [kN]	d_{ULS} [mm]	F_I [kN]	$d_{CLS,I}$ [mm]	$d_{CLS,I}/d_{ULS}$
8TPVB	20.0	49.2	6.15	59.2	1.2
8TDG	27.5	25.7	6.05	51.5	2.1
8TSG	34.3	34.5	6.59	56.1	1.7
10TSG	48.5	24.6	14.3	55.5	2.2

3.2.2 Configuration II

Configuration II (Fig. 9) is obtained by flipping the deformed shape obtained after the tests on configuration 0. For this reason, in this configuration the plate had a curvature opposite to the load direction. In Fig. 10 a direct comparison between the response in term of force-displacement graph of the considered specimens is depicted. Due to the deformed shape, an initial load was needed to flatten the LG plates. All the specimens were characterized by an initial non-linear behavior, due to the transition phase in which the glass fragments tend to fill the internal gap generated after the fracture. Once this gap is filled the behavior of the PDLG became quite linear until the final collapse.

Figure 9. Lateral view of configuration II, top broken ply.

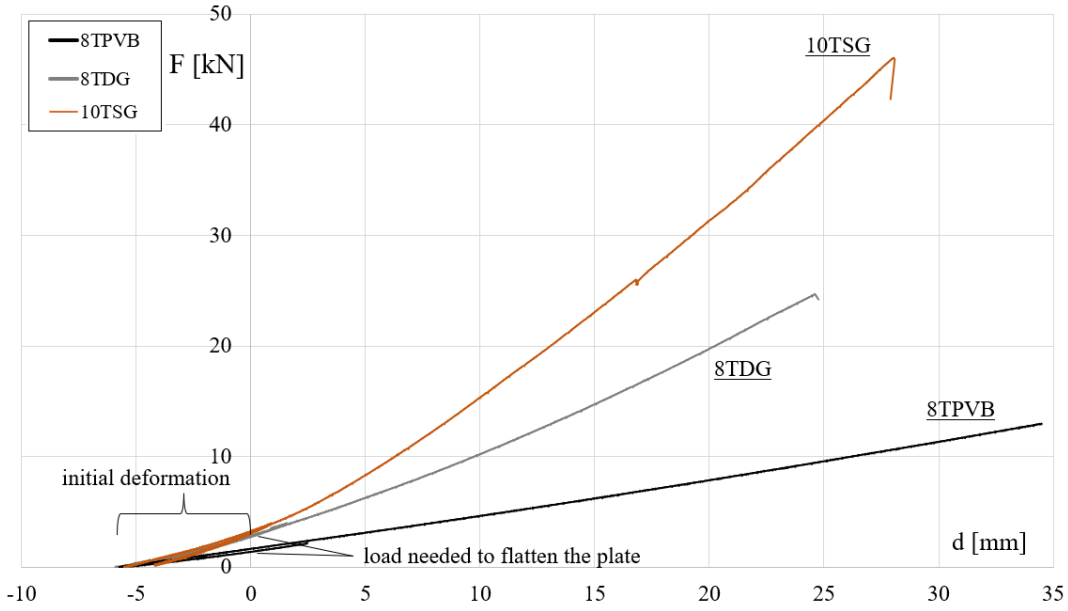

Figure 10. Comparison between the results on PDLG specimens with top ply damaged.

8TSG specimen had a problem with the instrumentation and for this reason its behavior is not represented. The response associated with PVB plate is more linear than the other cases and reach a greater global displacement. The initial load needed to flatten the plates is greater in the case of rigid

interlayers with respect the PVB one. In Tab. 6 the failure load of PDLG specimens with top ply glass damaged, $F_{II,}$ it is directly compared with the one that characterize the failure of the bottom ply glass in UDLG, F_0. Stiffer is the layer and closer is F_{II} to F_0. The failure load of the PVB case in configuration II is 1.5 lower than the undamaged one, on the contrary when DG41 and SG is considered the plates reached a similar failure load in undamaged and damaged configurations. Independently of the interlayer stiffness PDLG plates showed a good deformability in the post-breakage phase, $d_{CLS,II}$, being always the global displacement close to the one showed in configuration 0, d_{ULS}.

Table 6. Results obtained on PDLG specimens.

	UDLG		PDLG, Crack on top ply		
specimen name	F_0 [kN]	d_{ULS} [mm]	F_{II} [kN]	$d_{CLS,II}$ [mm]	F_0/F_{II}
8TPVB	20.0	49.2	13.18	34.6	1.51
8TDG	27.5	25.7	24.68	24.7	1.11
8TSG	34.3	34.5	*	*	*
10TSG	48.5	24.6	46.02	28.1	1.06

** instrument error*

3.2.3 Comparison

As a final summary between the results of the three tested configurations, Fig. 11 can be considered, in which the slope, i.e. the initial linear response of the force-displacement curve is depicted.

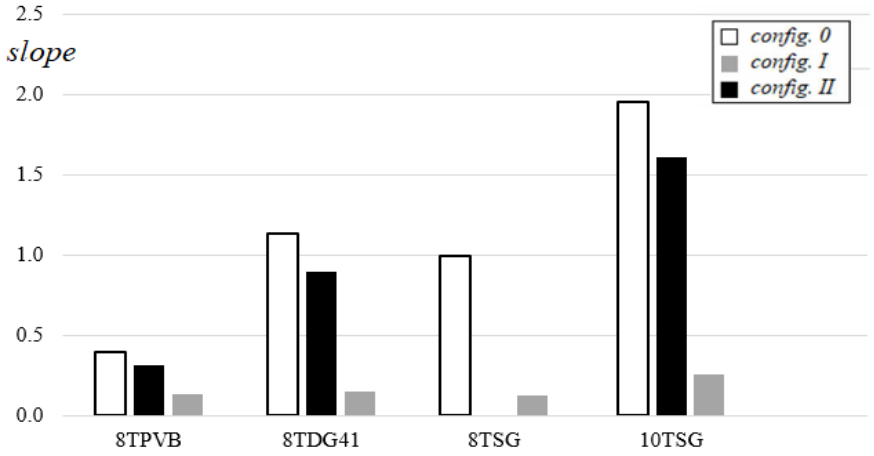

Figure 11. Comparison in terms of slope between all the considered specimens.

The three considered configurations are characterized by a remarkably different response. The PDLG specimens always present a lower stiffness than the UDLG ones. In particular, the decrement of stiffness for the PDLG with upper damage specimens is up to 57% (8TSG) with a mean value of 27%. On the contrary if PDLG with lower damage specimens are considered the decrement of stiffness ranges from 3 to 5 times the one of UDLG.

Finally, as a general view of the final failure, the global collapse of the 8TPVB LG plate, is sketched in Fig. 12. Despite at this stage the LG plate had no more carrying capacity and both plies were completely broke, the glass fragments remained glue to the interlayer without scatter all around, confirming the efficiency of the lamination processes.

Figure 12. Global failure of the 8TPVB specimen in configuration II.

4. Numerical modelling

Experimental tests were simulated by means the use of ABAQUS, which is a well-known commercial finite element (FE) software. In particular, to reduce the computational time, only a planar mesh in simply support conditions, with a concentrated force in the middle, was considered (Fig. 13). Element CPS with 8 nodes was used, for a total of 473000 elements with a maximum size of 0.5x0.5mm.

Simulating the simply support condition, vertical displacements (u_y) were hampered in both ends while horizontal the displacement (u_x) was fixed only on one end.

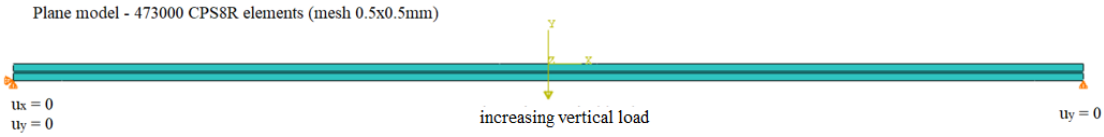

Figure 13. View of the planar finite element model.

4.1 UDLG models

For the model calibration in undamaged condition, a linear analysis was performed. The obtained numerical results are compared with the experimental one in Fig. 14. Since linear analyses were conducted on this stage, the glass and the interlayers were considered as linear material: the elastic modulus of the interlayers were assumed as the ones reported in Tab. 1, second row. The analyses were manually interrupted when the experimental failure loads, F_0, were reached. At this level the obtained displacements were compared with the experimental results to understand the accuracy of the models.

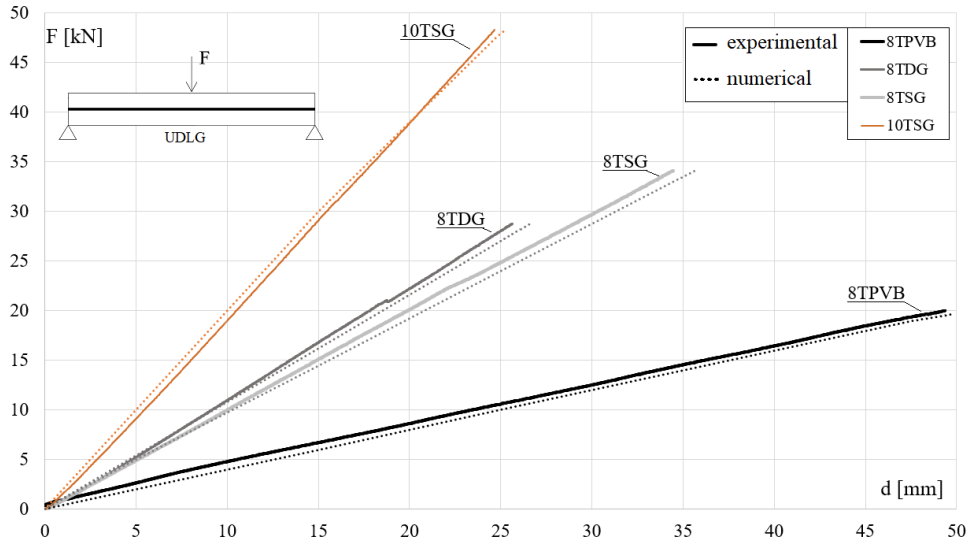

Figure 14. Comparison between numerical and experimental results obtained on UDLG specimens.

It can be noted the good agreement, in term of global stiffness, between numerical and experimental responses. From the numerical models it should be interesting to carrying out normal and tangential

stresses at the most stressed section of the plate. In particular, by referring to the ultimate point of the force-displacement curve, a direct comparison can be made between model with stiff and flexible interlayers (DG41 and PVB). In Figs. 15 and 16 normal (σ or S11) and tangential (τ or S12) stress distribution is proposed for 8TPVB and 8TDG specimens, respectively.

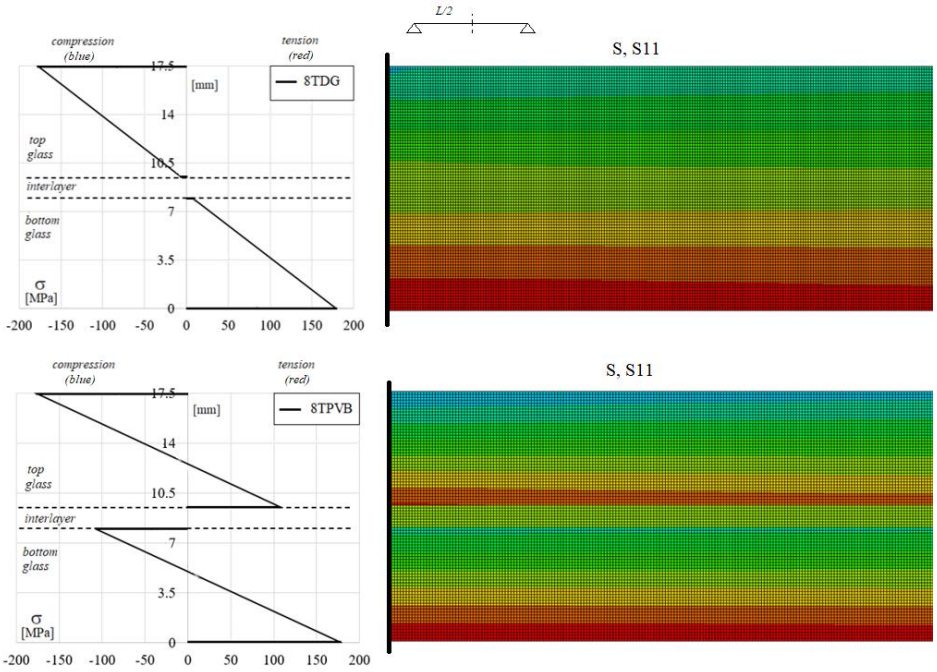

Figure 15. Normal stresses distribution on undamaged 8TDG and 8TPVB specimens (mid-section).

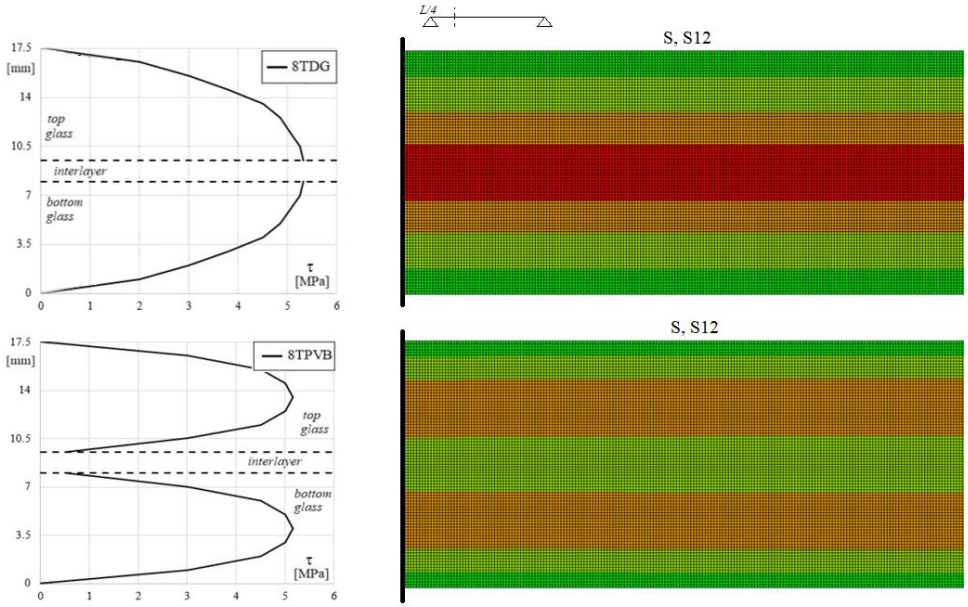

Figure 16. Tangential stresses distribution on undamaged 8TDG and 8TPVB specimens (quarter).

It is confirmed that, for the considered length and boundary conditions, the plates with PVB interlayer behaves close to the *layered* response, otherwise DG41 is stiff enough to guarantee a *monolithic* behavior. The values of the normal stresses are in agreement with the ones estimated with the EET method and discussed in Tab. 4.

4.2 PDLG models in configuration I

The post-breakage response of specimens in configuration I, was simulated by using two different techniques: i) introducing an equivalent variation of temperature and ii) using of a suitably calibrated elasto-brittle constitutive law (Hillerborg model). Another possible technique could be the deletion, of some portions of the mesh from the broken ply, simulating isolated fragments. The latter strategy is not herein discussed but will be used to introduce the stresses distribution after the breakage in section 4.2.3.

4.2.1. Equivalent Temperature

For undamaged tempered glass, compressive and tensile force, due to the tempering process, are in equilibrium: the outer surface of glass is plane and each portion exchanges equal and opposite actions with all neighboring ones. During the loading phase the linear stress distribution, which is generating through the plies, is added to the initial state of stress. The cracks start as soon as the outer compressive stresses are absorbed and overcome from the tensile one. Due to the elastic behavior of glass, when the glass fails, fragments release part of the stored mechanical energy by expanding at the edges, releasing compressive stresses, and contracting in the central part, releasing tensile stresses (Fig. 17). The number and the size of the glass fragments (Fig. 18) directly depended on the thermal tempering process (and hence on the initial state of stress) [22,23]. With an interlayer having good adhesion, which can keep fragments from scattering (as the SG one), the fractured glass ply tends to expand in its own plane. In the tested specimens this expansion was bounded by constraints, generating a residual out-of-plane deformation of the plates (Fig. 19).

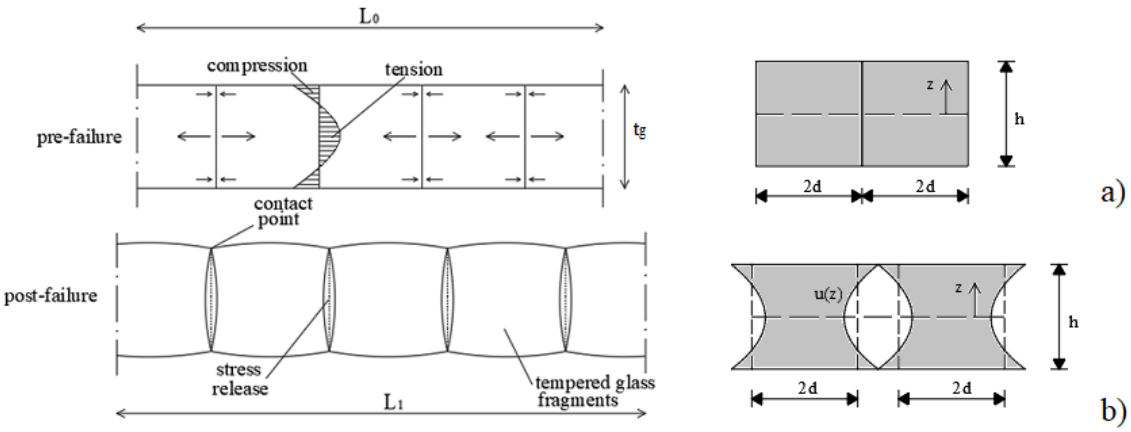

Figure 17. Tempered glass ply: a) residual stresses and b) deformation after breakage.

The displacements, *u*, generating between the fragments could be conventionally estimated with the equation:

$$u(z) = \frac{\sigma_{cT}}{E}\left[1 - \left(\frac{z}{h}\right)^2\right] s \qquad (3)$$

where σ_{cT} is the maximum tensile normal stress which can be reached in the glass, E is the Young modulus, *s* is half-length of the characteristic fragment. The *eigenstrain*, ε, due to the fragmentation of the tempered glass can be estimated from the knowledge of both the specimen size and the average value of the fragments and hence of the number of the fragments, n_f.

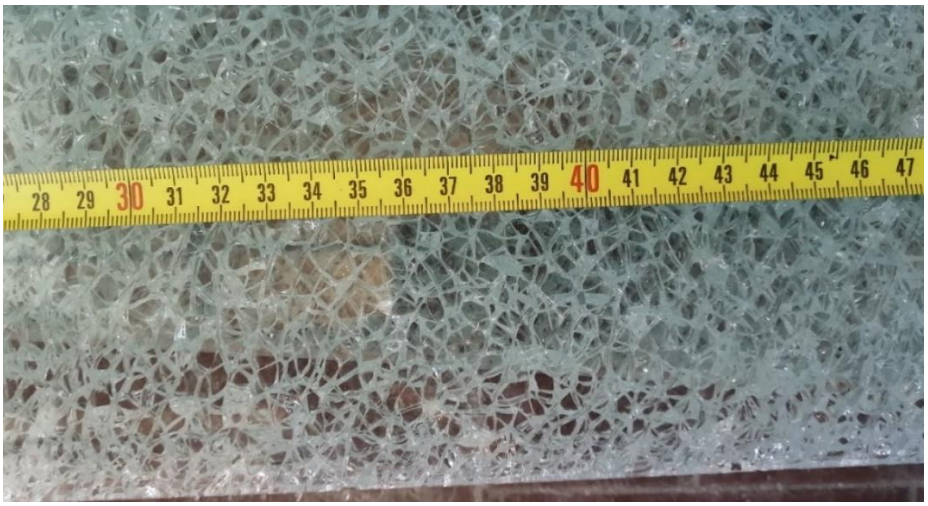

Figure 18. Zoom on a cracked ply.

It should be remarked that, the precise estimation of the characteristic length of the fragments is a complex problem, which should be based on a refined statistical evaluation of the fracture pattern [23]. The total expansion can be numerically replicated by a suitably calibrated equivalent thermal load ΔT (Fig. 19) uniformly distributed along the thickness of the glass ply:

$$\varepsilon = n_f \cdot u(\frac{h}{2}) = \Delta T \cdot \alpha_g \quad (4)$$

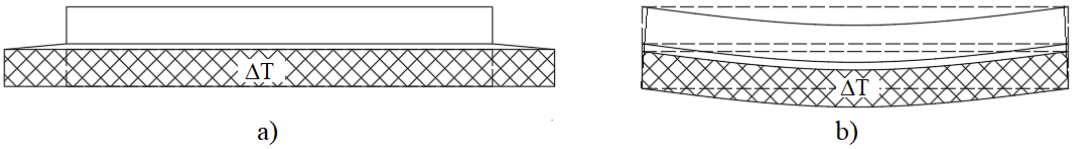

Figure 19. Temperature change to simulate an equivalent eigenstrain: a) free expansion b) flexure due to a restrained expansion.

In eq. 4) with α_g is indicated the thermal expansion coefficient of glass which is conventionally assumed equal to 9 10^{-6} °C^{-1}. This equivalent temperature produces an initial deformation of the considered models. Together with the ΔT, the Young modulus of the broken ply was decreased, E_{gI}, according to previous study [4]. The equivalent thermal distribution permits to predict the effects of shear and normal stresses transferred through interlayers from the broken ply to the undamaged one. The combination of thermal expansion and the presence of the broken ply produces a more flexible plate with respect to the initial undamaged one. The stiffer is the interlayer and the slightly lower is the ply expansion i.e. lower ΔT. Results obtained from the described procedure, are reported in Tab. 7 where the experimental data (F_I and $d_{CLS,I}$) are reported together with the Δ*T* value, the reduced Young modulus and the displacement reached by using the proposed procedure $d_{\Delta T}$.

Table 7. Results obtained from the equivalent temperature (ΔT) procedure, configuration I.

	PDLG, Crack on bottom ply				
specimen	F_I [kN]	$d_{CLS,I}$ [mm]	ΔT [°C]	E_{gI} [MPa]	$d_{\Delta T}$ [mm]
8TPVB	6.15	59.2	278	12.93	58.9
8TDG	6.05	51.5	210	24.77	48.8
8TSG	6.59	56.1	212	25.67	53.2
10TSG	14.3	55.5	198	33.12	50.7

It can be noted the good agreement between numerical and experimental findings, differences are lower than 10%. The procedure can be easily implemented and replicated on LG plates having different boundary conditions, length or number of plies. The time of analysis is quite limited because all the materials were assumed as linear.

4.2.2. Hillerborg constitutive law

The Hillerborg model is a suitably constitutive law implemented inside ABAQUS software which can account for the elastic-brittle behavior via the use of the *Brittle-Cracking material* option [24]. This model was originally developed for concrete and fragile materials (1976) and has been then used also for glass in a quite recent study [25]. In the software, its use is permitted only in the *explicit* module and for this reason the analyses were conducted under displacements control. Crack starts when the maximum principal stress reaches a specified tensile strength of the glass, i.e. the detection of the crack is based on the Rankine fracture criterion. When the criterion was met, the first crack is formed. The crack surface is normal to the direction of the maximum tensile principal stress. The width of the crack will increase until the work of the element reaches the inserted fracture energy. Moreover, during the crack also the shear stiffness, drop to zero in the crack plane at a prefixed opening displacement. Subsequent cracks could take place depending on the redistribution of the stresses on the glass layers. Cracking cannot be repristinated: once a crack occurs it remain for the duration of the analysis. On the other hand, crack closing and reopening is allowed. Since for the fracture energy the displacement at tensile failure cannot not be smaller than the displacement at crack initiation, there is an allowable element length $L_{e,max}$ for which the fracture energy can be represented correctly. The material, Hillerborg model, as implemented in ABAQUS, depends considerably on the element size, therefore it is always necessary to find the optimal compromise between the mesh dimension and the convergency of the results. When the element length is too big, the dissipation by damage is in general overestimated. As an example of the obtained results, Fig. 20 can be considered in which the 8TDG specimen is reported. The numerical deformed shape is sketched for different

displacement value (d) of the central section. It can be noted that at 27mm the maximum tensile stress was reached and the first breakage take place. The non-convergency of the analysis was reached at 48mm, when multiple cracks take place. In this model the interlayer material was implemented using exactly the non-linear material response depicted in Fig. 2.

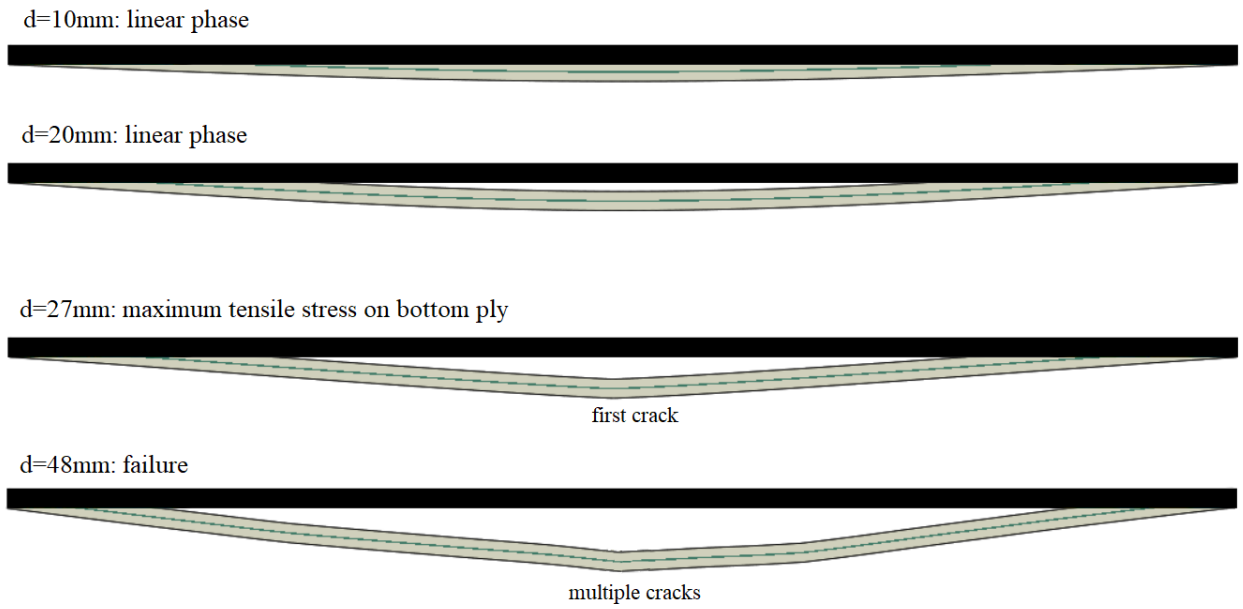

Figure 20. Results associated with Hillerborg constitutive law.

In Tab. 8 the results associated with configuration I are reported in term of collapse limit state load, $F_{0,H}$ and the associated vertical displacement ($d_{ULS,H}$). Since the analysis was under displacements control the force $F_{0,H}$ is given by the reactions on the supported points. After reached the first breakage, the analyses continued to run until the final non-convergency at displacement $d_{CLS,H.}$ This value could be compared with the experimental failure displacement ($d_{CLS,I}$).

Table 8. Results obtained with the Hilleborg model, configuration I.

	Experimental			Hilleborg model		
specimen name	F_0 [kN]	d_{ULS} [mm]	$d_{CLS,I}$ [mm]	$F_{0,H}$ [kN]	$d_{ULS,H}$ [mm]	$d_{CLS,H}$ [mm]
8TPVB	20.0	49.2	59.2	22	50	65
8TDG	27.5	25.7	51.5	29	27	48
8TSG	34.3	34.5	56.1	33	37	55
10TSG	48.5	24.6	55.5	49	27	52

The proposed method predicts accurately the first breakage of the LG plates in both term of force and maximum displacement. The post-breakage behavior is quite close with differences lower than 10%. If compared to the equivalent temperature method previously discussed, this kind of analysis is more precise but requires a greater amount of time from the computational standpoint. As previously discussed, the results obtained with this technique depends greatly on the mesh, on the setting of the crack opening parameters and on the elements type.

4.2.3. Stress distribution after breakage

After the crack opening the normal stresses drop to zero and the stresses are redistributed on the top layer. As an example, Fig. 21 shows the normal stress distribution on the 8TDG specimen after the first crack was opening.

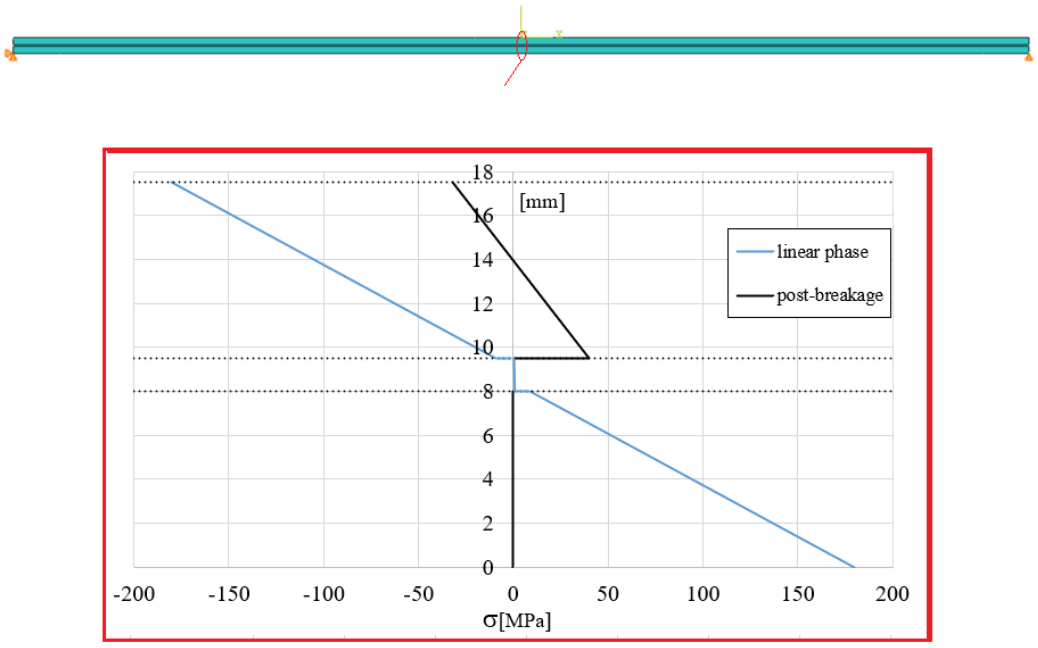

Figure 21. Normal stresses after the breakage on 8TDG.

As discussed, the breakage of the bottom glass ply cannot be numerically simulated just completely delete from the model the broken ply. In fact, the presence of fragments on the bottom layer and the stiffness of interlayer tends to stiffen the plate. The stresses can be still transfer between fragments and the interlayer depending on the stiffness of the interlayer itself. To demonstrate this effect a

simple model has been developed in which the fragments on the bottom ply have been directly modelled as small piece connected on the top to the interlayer. Looking into Fig. 22, from a simple linear analysis, it can be noted that if DG41 interlayer is considered the normal stresses are clearly visible passing from fragments to the polymeric material; otherwise, when PVB is implemented negligible stress transfer is present on the model.

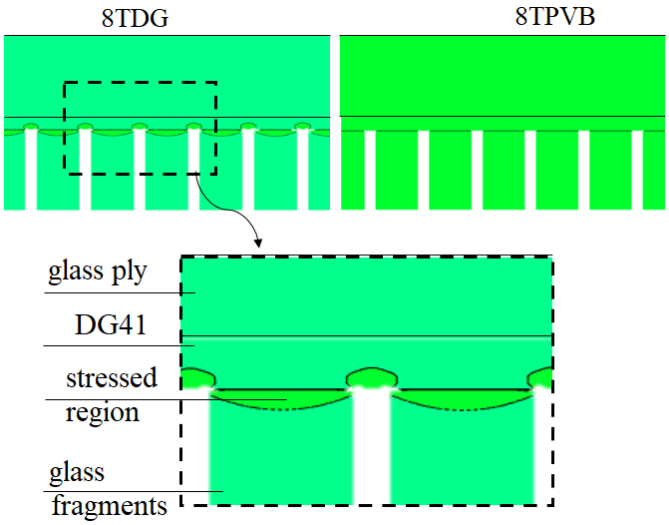

Figure 22. Stress volume stiffening the interlayer.

This effect represents a *tension stiffening* which contribute for rigid interlayer to stiff the LG also after the partial or total breakage of the glass ply.

4.3 PDLG models in configuration II

In configuration II the initial deformation is opposite to the load direction (Fig. 9) and the broken ply is in compression. An analytic model is proposed in Fig. 23a: at the beginning of the test (Stage 1), the top ply is cracked, and stresses can distribute only on the bottom ply. When the closest fragments touch each other, starting from the outer top face, a compression resultant is generated on the top ply, which became able to transfer normal stresses (Stage 2). Increasing the load, fragments on top are quite completely in touch and plate starts to behave close to the UDLG one (Stage 3). Finally, collapse is reached when tensile stresses cannot be carried on the bottom plate, similarly to what detected on UDLG (Stage 4).

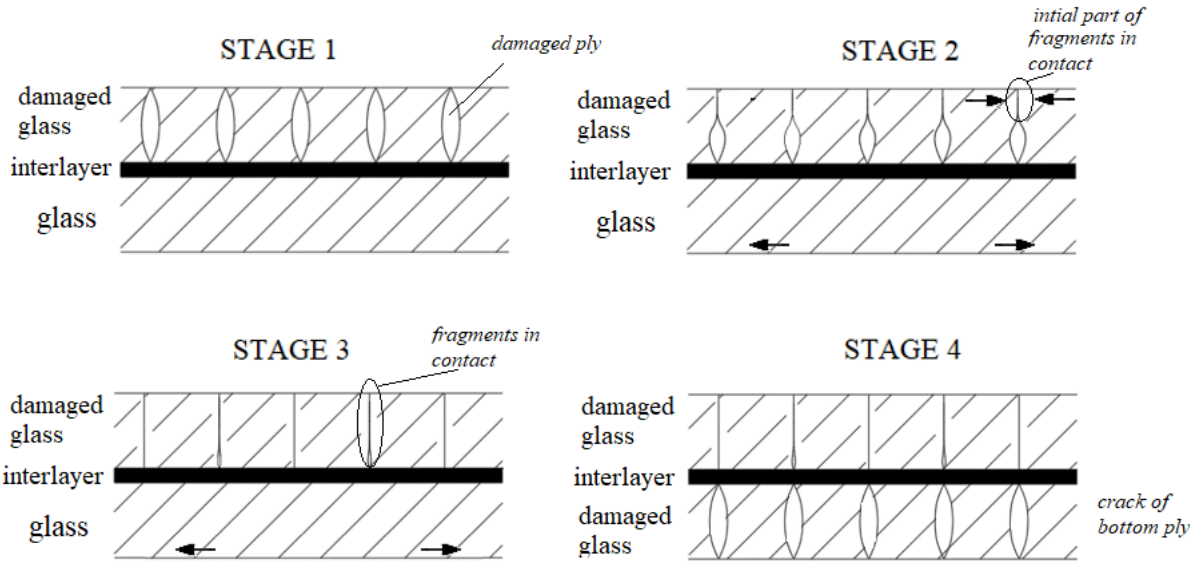

a)

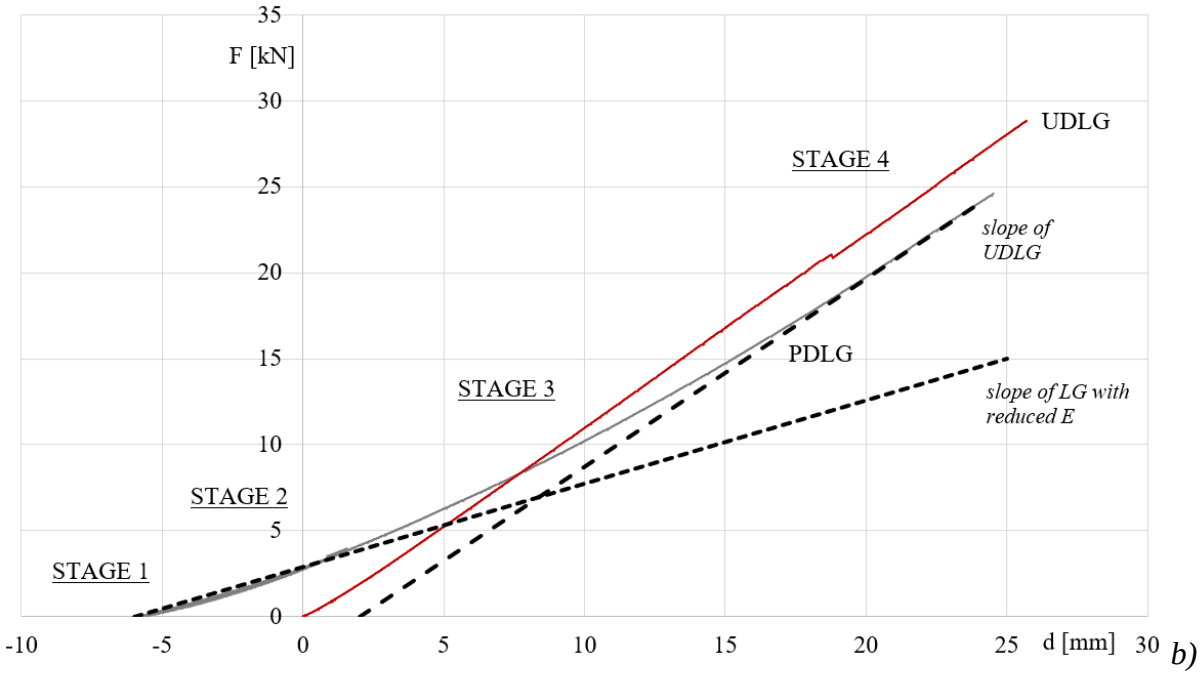

b)

Figure 23. Configuration II for 8TDG: a) different stages and b) force-displacement response.

The global response of 8TDG case is sketched in Fig. 23b. It can be noted that the curve is non-linear: the initial part of the curve can be simulated by using a reduced Young Modulus ($E_{g,I}$ in section 4.2.1) applied to the broken ply, while the final part of the curve has the slope close to the one which characterize the UDLG response. To reach the final failure load the same Hillerborg model previously

introduced was applied. The obtained results are reported in Tab. 9 in terms of experimental, F_{II}, and the numerical, $F_{II,H}$, failure loads. The failure load of bottom ply in UDLG case, F_0, with the associated displacement, d_{ULS} are reported too. It can be remarked that this modelling technique brings to non-negligible differences, up to 1.6 for PVB specimen.

Table 9. Numerical results obtained for configuration II.

	Experimental			Numerical
specimen name	F_0 [kN]	d_{ULS} [mm]	F_{II} [kN]	$F_{II,H}$ [kN]
8TPVB	20.0	49.2	13.18	22.4
8TDG	27.5	25.7	24.68	29.7
8TSG	34.3	34.5	*	37.4
10TSG	48.5	24.6	46.02	46.2

5. Parametric analyses

Starting from the previous ABAQUS undamaged models, parametric analyses have been developed to underline the influence of different geometric parameters on the global response of LG plates, which are of paramount importance in the structural design.

5.1 Size effect

The dimensions of the plate and the boundary conditions play an important role in the definition of the degree of coupling between the glass layers, as demonstrated with theoretical models in previous works [26]. To investigate the influence of this effect (called *size effect*), different values of the plate length (from 550mm to 6600mm) were considered. The range of variation was applied separately in the simply supported direction (Fig. 24a) and along the free ends (Fig. 24b).

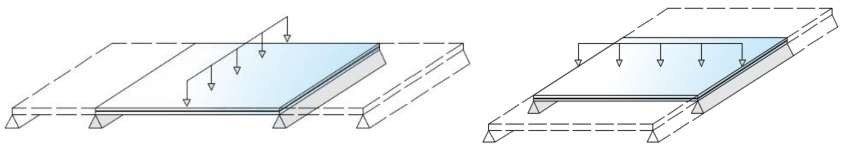

a) b)

Figure 24. Variation of distance for numerical analyses: a) supported direction b) free direction

Linear analyses were performed on 8TPVB and 8TDG plates monitoring the middle displacement. The ratio between the displacement obtained, at a prefixed load value, on the 8TDG (d_{DG}) and the one obtained with 8TPVB (d_{PVB}) is plotted in Fig. 25 for the considered cases.

It can be noted that, when the supports moves away from one another (Figs. 24a-25a), the influence of interlayer stifness on the vertical displacement decrease, i.e. d_{DG} / d_{PVB} ratio became closer to one. On the contrary, when the lenght change in the other direction, i.e. the supports maintain the same distance (Figs. 24b-25b), the ratio remain quite costant.

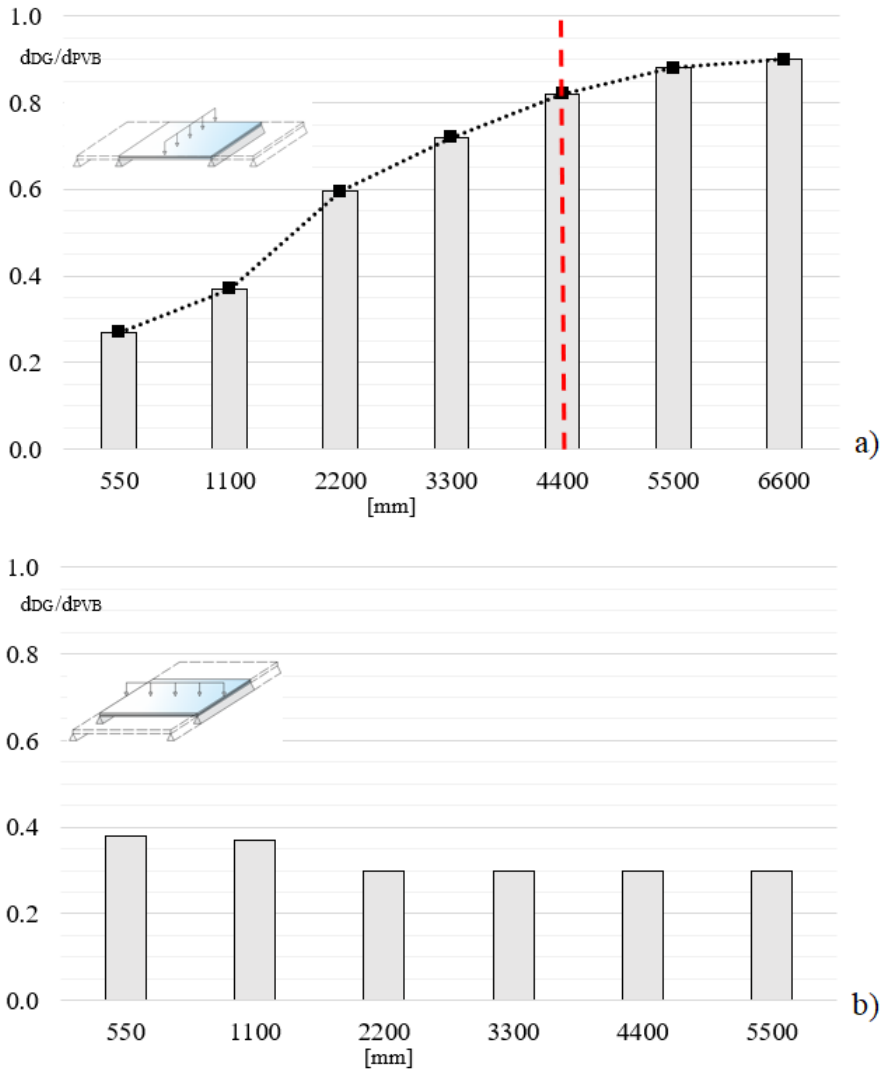

Figure 25. Size effect and definition of the critical length (vertical red dashed line).

The discussed result, confirmed also by a previous theoretical study [27], permits to identify a *critical lenght* (vertical dashed red line in Fig. 25). Starting from the *critical length* the plate behave as

monolitich indipendently of the interlaayer stiffness, therefore is not economical convient use stiff interlayer.

Looking into internal stresses (Fig. 26), it is confirmed that starting from the *critical length* no differences in the response of LG plates can be observed. In Fig. 26 normal and tangential stresses taken from the middle section of plates with length 500mm and 4400mm are reported. When the plate has a length of 4400 the behavior is *monolithic* and the use of different interlayer does not influence the degree of coupling of glass plies.

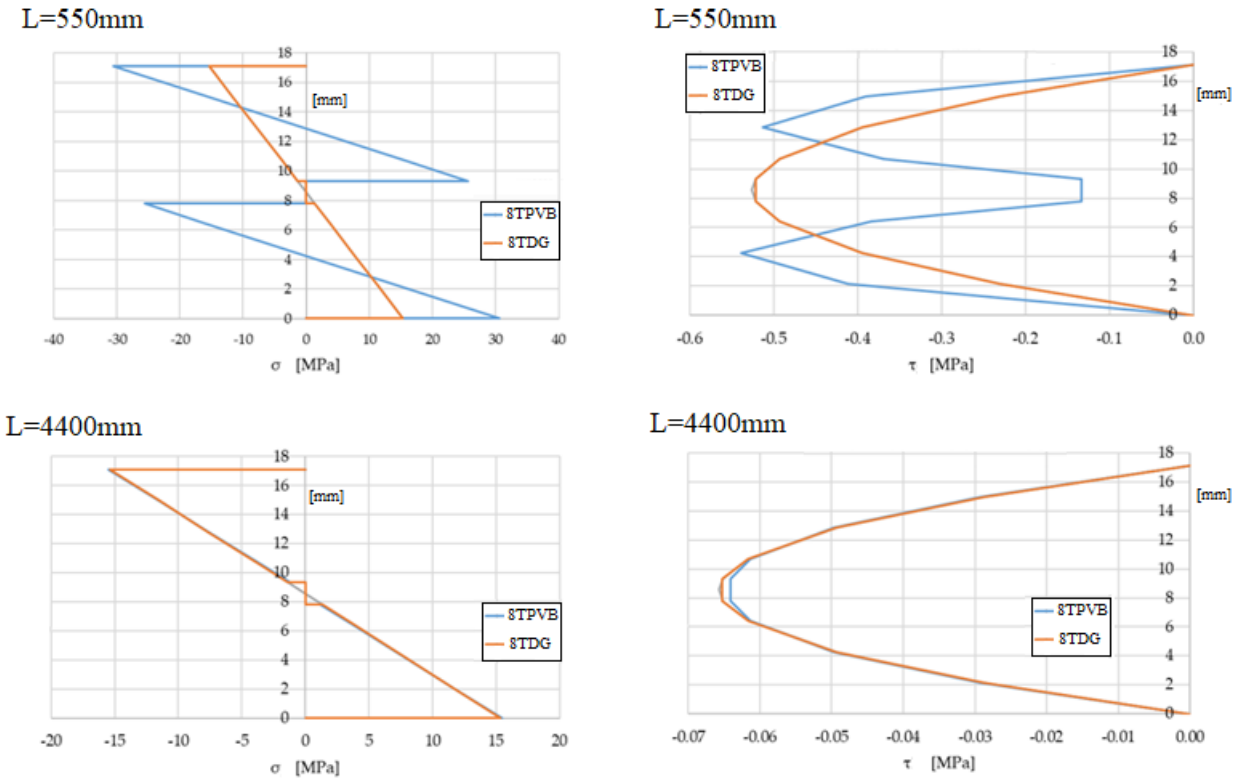

Figure 26. Comparison between numerical normal and tangential stresses in the mid-section.

The above mentioned behaviour should be always considered during the design phase of a glass structural element, cosidering that the cost of LG plates made by DG41 interlayer is about 3 times the ones made by PVB.

5.2 influence of interlayer thickness

Since the interlayer thickness affect the cost of the laminated plate, also this parameter was investigated. The considered interlayer thicknesses were 0.38, 0.76 and 1.52mm, according to the most used commercial products. As in the previous cases, 2-ply plates with 8mm tempered glass were taken into account, with the distance between the supports equal to 0.5m and 5.5m. PVB and DG41 interlayer were considered. Also, for these cases the linear analyses were performed monitoring the vertical displacement in the middle section. The ratio between the displacement obtained with each thickness over the one associated with the lowest ($d_i/d_{0.38}$) is plotted in Fig. 27.

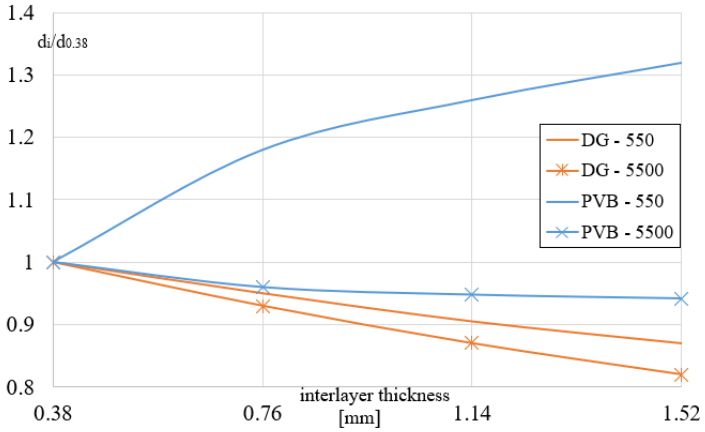

Figure 27. Interlayer thickness influence on the global response.

Considering the small specimen with PVB, increasing the interlayer thickness, the degree of coupling decrease, i.e. the global deflection increase. On the contrary, when the length is 5.5m the greater is the thickness of the interlayer, the lower is the value of the maximum displacement. For the stiff interlayer the trend is always the same independently of the specimen length, i.e. increasing the interlayer thickness, the overall stiffness increase too.

5.3 Influence of glass thickness

Starting from 8TDG and 8TPVB specimens (interlayer thickness equal to 1.52mm) the glass thickness was increased to 10 and 12mm. In Fig. 28 is reported the ratio between vertical displacement measured in the middle of 8TDG over the one associated with 8TPVB plates (d_{DG}/d_{PVB}). It can be

noted that, for the considered boundary conditions, the *critical length* is not dependent on the glass thickness.

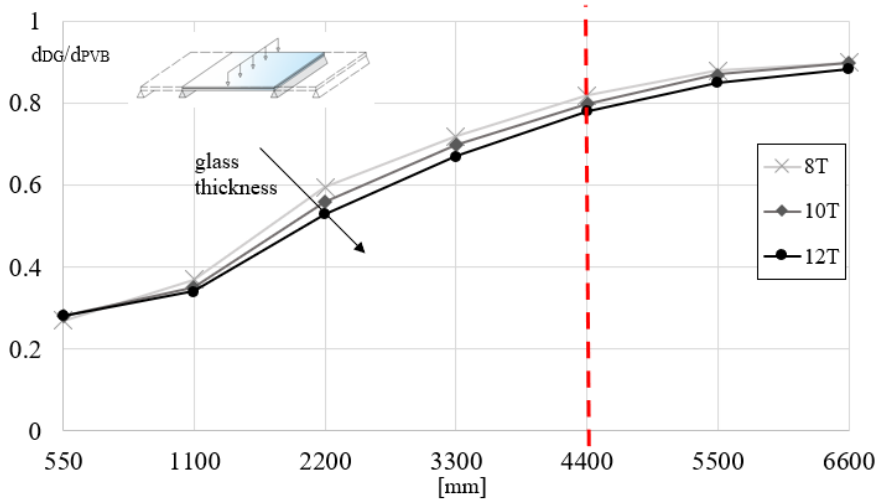

Figure 28. Glass thickness influence on the the definition of the critical length (vertical red dashed line).

5.4 The effect of additional layers

Finally, an additional layer of glass and polymeric film, was considered, generating 3-ply LG plates. The thickness of glass was 8mm and the interlayers were 1.52mm thick. Also, for these cases DG41 and PVB types were compared. In Fig. 29 the ratio between vertical displacement measured in the middle of the DG41 over the one on PVB plates (d_{DG}/d_{PVB}) is reported.

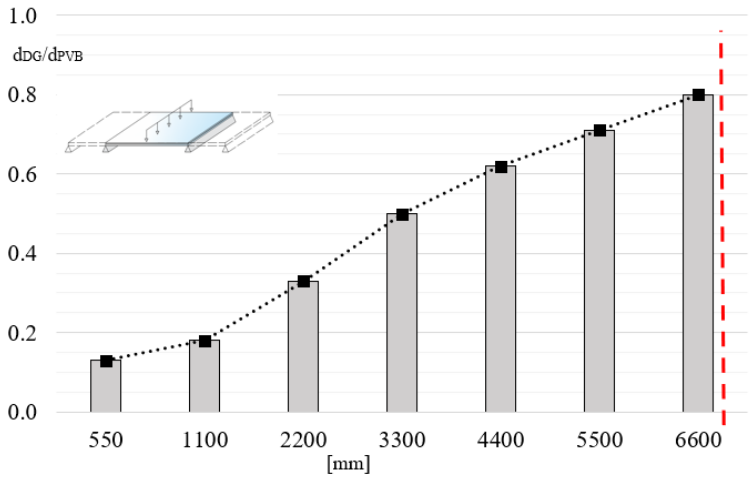

Figure 29. Size effect in 3-ply LG plates and definition of the critical length (vertical red dashed line).

The value of the *critical length* in the 3-ply case increases with respect the 2-ply case, i.e. an additional layer of glass increases the influence of the interlayer stiffness on the overall response.

Finally, according to previous experimental results [27], also for 3-ply case the post-breakage response is greatly depended on which ply of glass breaks first, as showed in the force-displacement graph plotted in Fig. 30. By comparing the global response to the undamaged one (red line in figure) when the bottom ply broke the stiffness reduction is 40% respect to the undamaged ones. In addition, if the central ply broke together with the bottom one, the residual global stiffness is almost 6% of the undamaged one. Otherwise, if only the central ply is broken the response is very close to the undamaged one. Lastly, with the breakage of the central ply together with the top one, the stiffness is almost 45% of the initial one. These results underline that due to the great non-linearity on the post-breakage behavior of LG plates, the superimposition of the effects cannot be used. The global response cannot be simulated considering only the final configuration, but it is important also to consider the intermediated stage, considering in which order the glass plies fails.

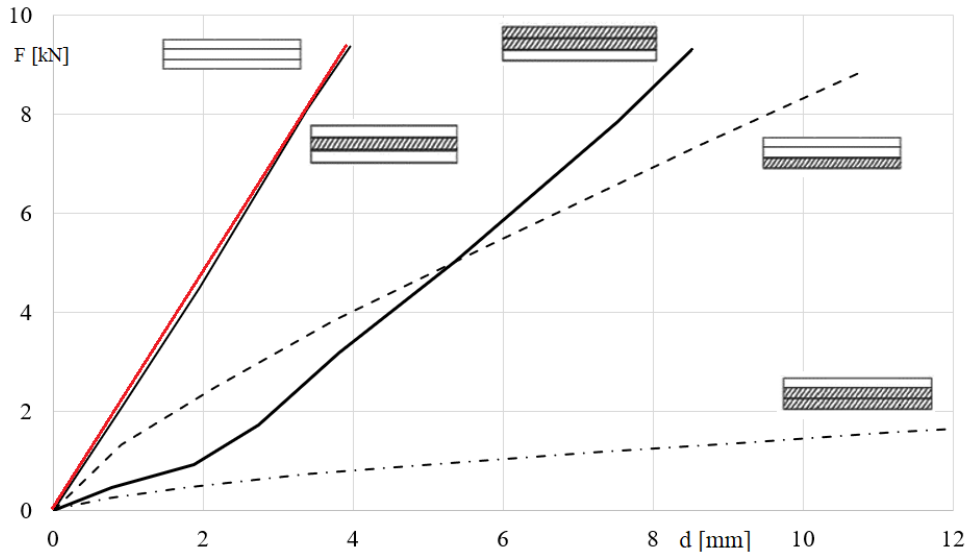

Figure 30. Experimental response of 3-ply LG plate with different damage path.

It can be noted that, in Fig. 30, only four failure scenarios were presented; to cover all the possible post-failure configurations for the 3-ply LG, it should be carried out a more extensive experimental campaign or it should be used a statistical/theoretical approach as discussed in ref. [28].

6. Concluding remarks

In the paper, the post-failure response of 2-ply LG plates was investigated through experimental tests and numerical models at different damage levels. Fully tempered glass with different ply thickness (10 and 8 mm) and different interlayers (PVB, DG41 and SG) were considered. Experimental tests were executed on simply supported LG plates loaded in the middle cross-section. Firstly, the influence of different interlayers on the stiffness of undamaged plates (configuration 0) was discussed. In this configuration the load was increased until the collapse of the bottom glass ply. Then, two additional configurations were tested: configuration I with the broken ply on the bottom and configuration II with the broken ply on the top. The LG response in configuration I is influenced by two factors: i) dimensions of the fragments in the broken ply and ii) stiffness of the interlayer. Considering the contribution of these two factors, plates with DG41 and SG showed a greater post-breakage capacity with respect the ones with PVB. From a structural standpoint, the use of a rigid interlayer permits hence to guarantee a safer post-failure response of the plates, which is a parameter of a paramount importance in the design. Focussing attention on configuration II, with the broken glass ply located on the top, the response changes completely with respect to the previous case. In this case the broken ply is in compression and the forces generated ensure a good response to the plates, which reached high failure loads and displacements, close to the ones registered on the undamaged specimens. It is important to underline that the beahvior of the plates is strictly depended on the boundary conditions.

The experimental results were then simulated by means the use of ABAQUS software. In particular, the undamaged behavior was simulated via simplified linear models, which permit to capture accurately the response. Otherwise, for the simulation of post-breakage response, more complex

modelling strategies were followed. Configuration I was simulated by means two different models: a) the equivalent temperature method, which was a linear analysis with an equivalent thermal uniform distribution used to simulate the expansion of the glass ply after the breakage; b) the use of an elasto-brittle constitutive law. The discussed techniques, once properly calibrated, were able to match the experimental results.

Finally, parametric analyses were presented to show the influence on the global response of:

i) Plate geometry (*size effect*). Plates with different dimensions were investigated, having the length from 550mm to 6600mm. Numerical findings were used to define a *critical length* from which the plates behave as *monolithic*, independently of the stiffness of the interlayer. The *critical length* could be used in the design phase, in order to reduce the costs of LG elements.

ii) Interlayer thickness. Three thicknesses (0.38, 0.76 and 1.52mm) were considered, analysing two different interlayer types. When a rigid interlayer (DG41) was used, the global stiffness increase with the increasing of the interlayer thickness. On the contrary, when PVB interlayer was used, the global behavior was strictly dependent on the plate length. When a small plate is considered, the increase of the interlayer thickness generated a more flexible plate; otherwise, for a long plate, the behavior of the plate become the same as the one with DG41.

iii) Glass thickness. Three thicknesses (8, 10 and 12mm) were considered. The trend of the global response remains the same, i.e. the *size effect* was not directly influenced by the glass thickness.

iv) Additional glass ply (3-ply LG plate). An additional glass ply and interlayer was added forming the 3-ply LG plate. The *critical length* shifts, i.e. the *monolithic* behavior can be reached with greater length with respect to the 2-ply LG plates.

Finally, it can be remarked that a European Technical Working Group (TWG) is currently working on the develop of a new Eurocode entirely devoted to the glass as structural material. In view of this, the present paper brings additional useful and important information for the design of LG plates with different interlayer types. The correct definition of a *critical length* in the design phase can be of paramount importance, in view of an economical evaluation of the structural solution made by glass.

Acknowledgement

The authors are grateful to Eng. Federica Celada whose work for the Master thesis provided an important part of the results presented in this paper. Special thanks are due to Roberto Minerva and Daniele Spinelli (LPM, POLIMI) who supervised the student in setting up the experimental apparatus. The authors are also grateful for the efforts and for the detailed work made by the anonymous Reviewers which helped significantly in improving the quality of the paper.

CRediT authorship contribution statement

L.B. conceptualization of the work; L.B. supervision; M.S. numerical analyses; M.S. experimental activity and data elaboration; M.S. L.B. writing/review of the whole paper. All authors have read and agreed to the published version of the manuscript.

Declaration of Competing Interest

The authors declare that they have no known competing financial interests or personal relationships that could have appeared to influence the work reported in this paper.

References

1. Wurm J. Glass Structures: Design and Construction of Self-supporting Skins, *Birkhauser*; 2007.
2. CEN/TC 250. prCEN/TS 19100, Design of glass structures. European Committee for standardization 2021.

3. EN 1990: Eurocode: Basis of Structural Design, European Committee for standardization, 2002.
4. Biolzi L., Orlando M., Piscitelli L.R., Spinelli P. Static and dynamic response of progressively damaged ionoplast laminated glass beams. *Composite Structures* 157, 337-347, 2016. doi:10.1016/j.compstruct.2016.09.004.
5. Castori G., Speranzini E. Structural analysis of failure behavior of laminated glass. *Composites Part B: Engineering* 125, 89–99, 2017. doi:10.1016/j.compositesb.2017.05.062.
6. Foraboschi P. Optimal design of glass plates loaded transversally. *Mater Des.* 62, 443–58, 2014. doi:10.1016/j.matdes.2014.05.030.
7. Biolzi L., Cattaneo S., Orlando M., Piscitelli L.R., Spinelli P. Post-failure behavior of laminated glass beams using different interlayers. *Composite Structures* 202, 578–89, 2018. doi:10.1016/j.compstruct.2018.03.009.
8. Galuppi L, Royer-Carfagni G. A homogenized model for the post-breakage tensile behavior of laminated glass. *Composite Structures* 154, 600–15, 2016. doi:10.1016/j.compstruct.2016.07.052.
9. Biolzi L., Cattaneo S., Orlando M., Piscitelli L., Spinelli P., Constitutive relationships of different interlayer materials for laminated glass. *Composite Structures* 244, 112221, 2020. doi:10.1016/j.compstruct.2020.112221.
10. Martín M., Centelles X., Solé A., Barreneche C., Fernández A.I., Cabeza L.F. Polymeric interlayer materials for laminated glass: a review. *Constr. Build. Mater.* 230, 116897, 2020. doi:10.1016/j.conbuildmat.2019.116897.
11. Bennison S.J., Qin MHX, Davies PS. High-performance laminated glass for structurally efficient glazing. Innov Light Struct Sustain Facades, Hong Kong, p. 1–12, 2008.
12. Alvarez G, Flores JJ, Aguilar JO, Gómez-Daza O, Estrada CA, Nair MTS, et al. Spectrally selective laminated glazing consisting of solar control and heat mirror coated glass:

preparation, characterization and modelling of heat transfer. *Sol Energy* 78, 113–24, 2005. doi:10.1016/j.solener.2004.06.021.

13. Galuppi L., Royer-Carfagni G., Enhanced Effective Thickness for laminated glass beams and plates under torsion, *Engineering Structures* 206, 110077, 2019. doi:10.1016/j.engstruct.2019.110077.
14. Lopez-Aenlle M., Pelayo F., Fernandez-Canteli A., Garcia Prieto M.A., The effective-thickness concept in laminated-glass elements under static load, *Engineering structures* 56, 1092-1102, 2013 doi:10.1016/j.engstruct.2013.06.018.
15. ASTM D638-14, Standard Test Method for Tensile Properties of Plastics. West Conshohocken, PA, 2014. doi:10.1520/D0638-14.
16. International Organization for Standardization. ISO 527:2012 Plastics - Determination of tensile properties. Genève, CH: 2012.
17. Ferry JD. Viscoelastic Properties of Polymers. New York: 1980. doi:10.1080/00914037208075296.
18. Biolzi, L., Bonati, A., Cattaneo, S. Laminated Glass Cantilevered Plates under Static and Impact Loading, *Advances in Civil Engineering*, 7874618, 2018. doi:10.1155/2018/787461.
19. Galuppi L., Royer-Carfagni G., Effective thickness of laminated glass beams: New expression via a variational approach. *Engineering Structures* 38, 53-67, 2012. doi:10.1016/j.engstruct.2011.12.039.
20. Langosch K., Feldmann M. VSG-Glasstutzen unter kombinierter Langzeit- und Kurzzeitbelastung. *Stahlbau* 81, 149-158, 2012. doi:10.1002/stab.201290059.
21. Feldmann M., Langosch K. Zum Biegeverhalten von VSG-Laminaten unter Quer-order Langsbelastung. *Stahlbau* 80, 52-60, 2011. doi: 10.1002/stab.201120007.
22. Pourmoghaddam N., Kraus M.A., Schneider J., Siebert G. Relationship between strain energy and fracture pattern morphology of thermally tempered glass for prediction of the 2D macro-

scale fragmentation of glass. *Glass Struct. Eng*. 4, 257-275, 2019. doi:10.1007/s40940-018-0091-1.

23. Pourmoghaddam N., Schneider J. Experimental investigation into the fragment size of tempered glass. *Glass Struct. Eng.* 3(2), 167–181, 2018b. doi:10.1007/s40940-018-0062-0.
24. Hillerborg A. Fracture mechanics concepts applied to moment capacity of reinforced concrete beams. *Engineering Fracture mechanics* 35 (11), 233-240, 1990. doi:10.1016/0013-7944(90)90201-Q.
25. Pelfrene J., Van Dam S., Sevenois R., Gilabert F., Van Paepegem W. Fracture simulation of structural glass by element deletion in explicit FEM. Proccedings of Challenging Glass 5 – Conference on Architectural and structural applications of glass. Ghent, Belgium, June 2016.
26. Galuppi L., Royer-Carfagni G., The effective thickness of laminated glass: inconsistency of the formulation in a proposal of EN-standards. *Composites Part B: Engineering* 55, 109-118, 2013. doi:10.1016/j.compositesb.2013.05.025
27. Biolzi L., Casolo S., Orlando M., Tateo V. Modelling the response of a laminated tempered glass for different configurations of damage by a rigid body spring model. *Engineering Fracture Mechanics* 218, 106596, 2019. doi:10.1016/j.engfracmech.2019.106596
28. Bonati, A., Pisano, G., Royer-Carfagni, G. Probabilistic considerations about the strength of laminated annealed float glass. *Glass Structures & Engineering* 5(1), 27-40, 2020. doi:10.1007/s40940-019-00111-8.